inventions

MDPI

Article

Thermodynamic Analysis of Binary and Trinary Power Cycles Fueled with Methane–Hydrogen Blends

Vladimir Kindra [1,*], Nikolay Rogalev [2], Andrey Rogalev [1], Olga Zlyvko [1] and Maksim Oparin [1]

[1] Department of Innovative Technologies of High-Tech Industries, National Research University "Moscow Power Engineering Institute", 111250 Moscow, Russia
[2] Department of Thermal Power Plants, National Research University "Moscow Power Engineering Institute", Krasnokazarmennaya St. 14, 111250 Moscow, Russia
* Correspondence: kindra.vladimir@yandex.ru

Abstract: The development of hydrogen energetics is a possible way to reduce emissions of harmful substances into the atmosphere in the production of electricity. Its implementation requires the introduction of energy facilities capable of operating on environmentally safe fuel. At the same time, from a technological point of view, it is easier to implement a gradual shift to the use of hydrogen in power plants by burning methane–hydrogen blends. This paper presents the results of thermodynamic studies of the influence of the chemical composition of the methane–hydrogen blend on the performance of binary and trinary power units. It is shown that an increase in the hydrogen volume fraction in the fuel blend from 0 to 80% leads to a decrease in the Wobbe index by 16% and an increase in the power plant auxiliaries by almost 3.5 times. The use of a trinary CCGT unit with a single-circuit WHB and working fluid water condensation makes it possible to increase the net efficiency by 0.74% compared to a binary CCGT with a double-circuit WHB and a condensate gas heater.

Keywords: thermodynamic cycle; heat exchanger; hydraulic loss; heat transfer surface; energy efficiency

Citation: Kindra, V.; Rogalev, N.; Rogalev, A.; Zlyvko, O.; Oparin, M. Thermodynamic Analysis of Binary and Trinary Power Cycles Fueled with Methane–Hydrogen Blends. *Inventions* **2022**, *7*, 73. https://doi.org/10.3390/inventions7030073

Academic Editors: Umberto Lucia, Debora Fino and Giulia Grisolia

Received: 29 July 2022
Accepted: 23 August 2022
Published: 30 August 2022

1. Introduction

Currently, one of the main global trends in the development of the energy industry is the shift to renewable energy resources (RES). Wind and solar power plants are widely used. At the moment, the total generation of electricity using RES in the world is only 3% [1,2]. However, in the next few decades, many European countries, Japan, the USA, Canada, and China are planning to significantly increase this number in order to reduce emissions of toxic substances and greenhouse gases in the production of electricity [3,4]. To implement such a large-scale ambitious task, it will be necessary to create storage systems that ensure the alignment of energy production and consumption schedules [5,6]. The structure of existing energy systems will be subject to significant transformation.

One of the possible scenarios for the energy industry development is the shift to hydrogen energetics [7–9]. A popular concept implies the production of hydrogen from renewable energy resources during off-peak loads, followed by effective utilization of the stored energy. It is possible to transport hydrogen from the place of production to the place of consumption through existing gas pipelines [10,11]: hydrogen will be mixed with natural gas. Further the fuel blend can be sent to thermal power plants for subsequent combustion to generate electricity.

Since the cost of hydrogen produced according to the technology described above will be significant, it is advisable to carry out its subsequent combustion at the most efficient CCGT units. There is a number of ways to improve CCGT unit efficiency. Most of the known ways provide an increase in the electrical network efficiency by 0.6–3.6%. Their implementation usually requires capital cost increases, and sometimes the maneuverability

and reliability of the power facility suffers. Therefore, the implementation of various methods or their combinations is not always economically feasible.

The basic method for increasing CCGT efficiency is to increase the initial temperature of the gas turbine cycle. Thus, an increase in the temperature at the gas turbine inlet (TIT) by 100 °C leads to an increase in the power unit efficiency by 0.9–1.5% [12]. It is worth remarking that the available nickel alloys can operate at temperatures below 900 °C, and the cooling system efficiencies are close to their limits [13]. In this regard, a further increase in CCGT useful electrical efficiency by increasing the GTU initial temperature is problematic.

An alternative approach to increasing CCGT efficiency is to increase the degree of flue gas heat utilization. In particular, increasing the pressure of the heat carrier in the waste heat boiler increases the heat recovery efficiency and, thus, increases the net generation of electricity in the steam turbine plant [14]. In addition, it is possible to use superheating to improve energy efficiency [15]. Increasing the heat carrier pressure and introducing reheating can reduce heat carrier thermal potential loss.

The introduction of an additional pressure circuit in the waste heat boiler with lower parameters makes it possible to efficiently utilize supplementary heat [16]. The maximum amount of recuperated heat in this case is limited by the minimum flue gas temperature, which is determined by the condition of steam saturation and low-temperature corrosion of the rear heat recovery surfaces in the presence of sulfur in the fuel, as well as the waste heat boiler efficiency.

A promising way to reduce flue gas losses for CCGT is the transition to trinary cycles, which are combined cycle gas turbine units with integrated circuits on low-boiling heat carriers [17]. For example, CCGTs with ORC are considered in the study by [18]. Through the use of NK-36ST GTU with a single-circuit waste heat boiler, the utilization of low-grade heat in the ORC makes it possible to achieve net CCGT efficiency of more than 60% at a cooling water temperature in the low-grade cycle below 0 °C.

The use of trinary cycles was also considered in the article by [19]. It was found in the work that the shift from a single-circuit CCGT to a three-circuit plant allows for increases in the electric power from 213.4 MW to 222.7 MW and increases in the net efficiency by 2.14%. The net efficiency of a trinary single-circuit power plant is 0.45% higher than that of a CCGT with a double-circuit waste heat boiler.

With an increase in the hydrogen volume fraction in the fuel, the concentration of water vapor in the exhaust gases also increases, which will increase the energy released during H_2O condensation. This energy can be usefully utilized in additional corrosion-resistant heating surfaces of the waste heat boiler, which will increase the plant efficiency.

The purpose of this work is to analyze the influence of the methane–hydrogen blend components ratio, as well as the structure of thermal circuits, on the main energy characteristics of binary and trinary units. To achieve this purpose, schematic solutions and mathematical models of CCGTs operating on a methane–hydrogen blend have been developed, with the use of which thermodynamic studies have also been carried out.

2. Materials and Methods

2.1. Binary and Trinary Thermal Schemes of CCGT on Methane–Hydrogen Blend

The object of this study was the thermal schemes of combined-cycle plants operating on a methane–hydrogen blend. To select the optimum alternative, three CCGT thermal schemes were considered:

- CCGT with a single-circuit waste heat boiler (Figure 1a),
- CCGT with a double-circuit waste heat boiler, and a superheating and condensate gas heater (CGH) (Figure 1b),
- CCGT with a single-circuit waste heat boiler, and an additional circuit on a low-boiling heat carrier (Figure 1c).

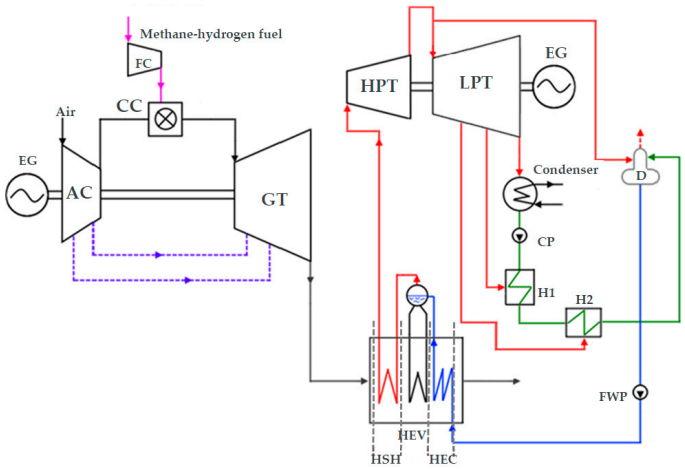

(**a**) with single-circuit WHB

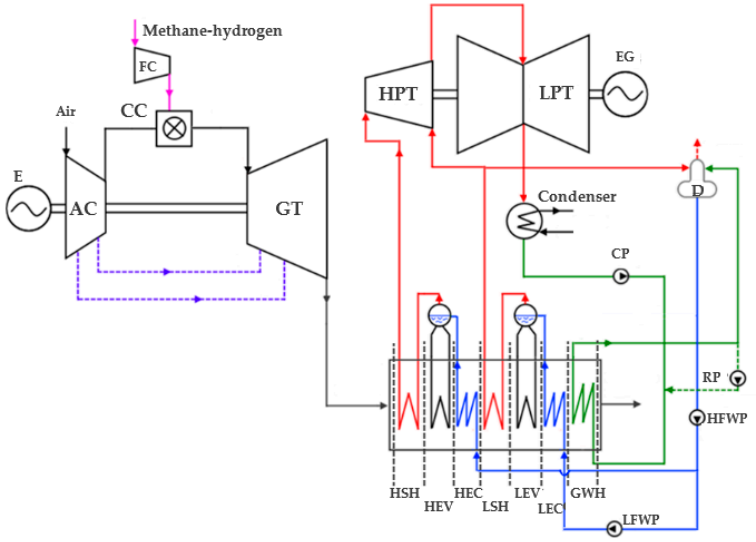

(**b**) with double-circuit WHB

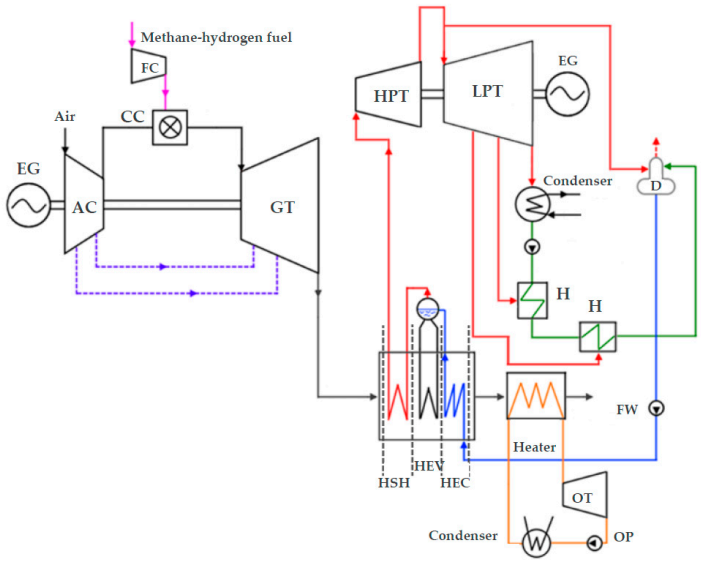

(**c**) with condensing heat exchanger

Figure 1. Combined cycle plant.

The technical characteristics for modeling a methane–hydrogen turbine are taken similarly to the domestic gas turbine GT-160 with an initial temperature of the working fluid equal to 1060 °C. It is assumed that the fuel mixture is fed to the CCGT through a gas line at a pressure of 0.7 MPa and a temperature of 15 °C and then increases its pressure by 2.5 MPa in the booster compressor.

Scheme 1 is presented in Figure 1a. The air enters the air compressor (AC), where it is compressed to 1.1 MPa. A small part of the compressed air is sent to cool the elements of the hot gas path of the gas turbine. The main part of the air enters the combustion chamber (CC). The fuel is compressed in a fuel compressor (FC) and fed to the CC. The released heat during the combustion process heats the working fluid to 1060 °C, which then enters the gas turbine inlet. The potential energy of high-temperature gas is spent on the rotation of the gas turbine rotor. The rotor is mounted on the shaft together with the first electric generator (EG). The gas turbine exhaust gas enters the waste heat steam generator that produces steam for the STP. In the waste heat boiler, the gas sequentially passes the heating surfaces of the superheater (HSH), evaporator (HEP), and economizer (HEC). The waste heat boiler exhaust gas is released into the atmosphere. The produced steam is directed to the high-pressure turbine (HPT) of the STP. After the steam has done useful work, part of it is sent to the deaerator (D). Most of the steam is sent to the low-pressure turbine (LPT) of the STP, where its heat drops and enters the condenser. The resulting condensate is sent to the electric condensate pump (CP). Preheated water is sent to the deaerator, heated by steam to saturation, cleaned of harmful non-condensable gases, and fed to the feed water pump (FWP) driven by an electric motor. The high-pressure water is sent to the economizer where it is heated to a temperature close to the saturation temperature. The water is then directed to the natural circulation evaporator drum. Saturated water from the drum passes over the surface of the evaporator, and part of it turns into steam. Then the steam–water mixture enters the drum, where the steam is separated. Saturated steam from the evaporator drum enters the superheater. The second electric generator is installed on the shaft of the steam turbine and generates electricity.

Based on the first scheme, a heat flow diagram for a double-circuit CCGT was developed (Figure 1b). The double-circuit scheme of the CCGT differs from the basic configuration by the use of high- and low-pressure feed pumps (HPFPs and LPFPs), an additional superheater (LSH), an evaporator (LEV), an economizer (LEC), and a gas water heater (GWH).

The use of trinary combined-cycle CCGT with corrosion-resistant condensing heat exchangers is a promising technical solution as well. In [19], it was found that it is favorable to use the organic Rankine cycle (ORC) with developed heat recovery in trinary CCGT. Heating the working fluid above the saturation parameters reduces the risk of moisture formation in the turbine flow path. However, excessive overheating can cause overheating of the output working fluid, which increases the average integral temperature of the heat sink. This factor can reduce the cycle thermal efficiency, which is why it is better to use ORC without thermal energy recovery by deep cooling of exhaust gases to the dew point temperature.

To utilize the low-grade heat of the CCGT exhaust gases, it is possible to form a power plant with a condensing corrosion-resistant heat exchanger (Figure 2). The trinary power plant consists of a GT, an STP, and a low-grade ORC plant. The organic Rankine cycle consists of an organic turbine (OT), a pump (OP), and a condenser. The input data for modeling the considered thermal schemes are presented in Table 1.

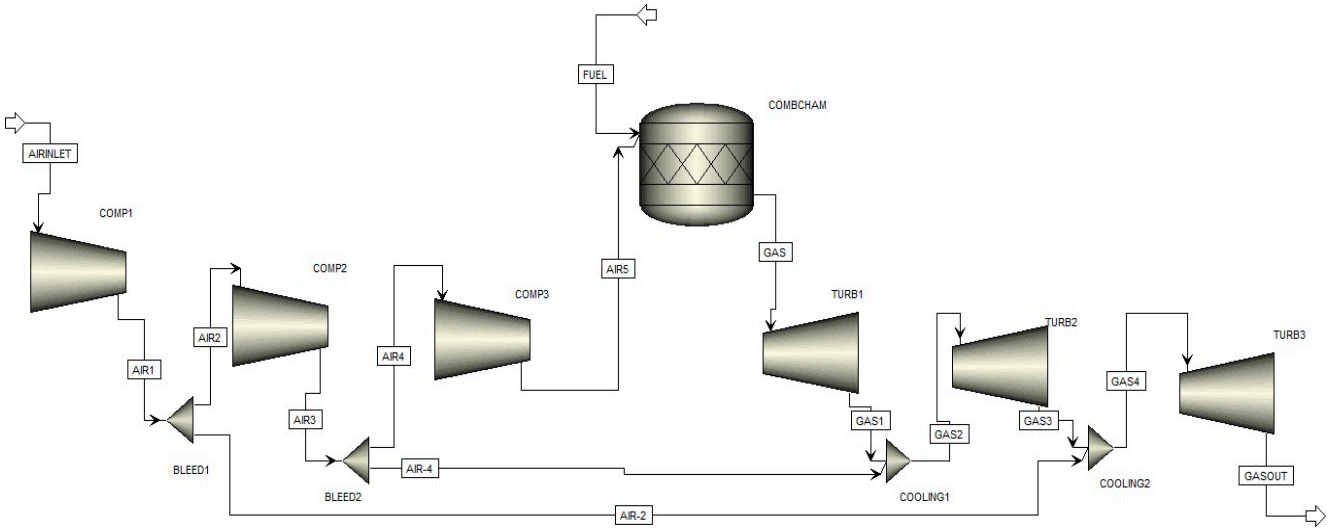

Figure 2. The cooled GTU scheme.

Table 1. Initial data for modeling ORC and CCGT on methane–hydrogen blend.

Parameter	Value
Initial data for modeling CCGT	
GT flue gas massflow, kg/s	509
GT initial temperature, °C	1060
GT pressure ratio	10.9
Exhaust gas temperature, °C	523.3
Fuel compressor internal relative efficiency, %	88
Steam turbine internal relative efficiency, %	90
Superheater hot end temperature difference, °C	20
HRSG maximum exit steam temperature, °C	560
Evaporator cold end temperature difference, °C	10
Economizer outlet water subcooling, °C	10
Deaerator inlet water subcooling, °C	10
Condenser temperature difference, °C	5
Cooling water temperature after the condenser, °C	25
Minimal heat carrier temperature at the HRSG inlet, °C	60
Minimal flue gas temperature at the HRSG exit, °C	80
Deaerator pressure, MPa	0.12
Pressure loss in superheater, %	5
Excess of pressure in deaerator extraction relative to deaerator pressure, %	40
Pressure loss between the condensate pump and deaerator, %	40
Internal efficiency of feed water and condensate pumps, %	85
Vapor fraction at the steam turbine exit, %	90
Mechanical efficiency, %	99
Electric motor and power generator efficiencies, %	99
Initial data for modeling ORC	
Minimal regenerator temperature difference, °C	5
Maximum temperature in the cycle, K	373.15
Minimum temperature in the cycle, K	303.15
Maximum pressure in the organic cycle, MPa	4.5
Minimum pressure in the organic cycle, MPa	1.43
Pump internal relative efficiency, %	85
Turbine internal relative efficiency, %	85
Power generator and electric motor efficiency, %	99
Mechanical efficiency, %	99

2.2. Mathematical Model of a Cooled Gas Turbine

To develop a mathematical model of a gas turbine, the AspenOne Plus software package was chosen. To create the same simulation conditions, the following parameters were fixed: the ratio of coolant flow rates to each compartment of the gas turbine, and the relative internal efficiencies of the compressor and turbine for all GTU (Table 2), as well as the initial temperature at the gas turbine inlet and the exhaust gas flow rate out of it for each GTU individually. The scheme of the mathematical model of the cooled GTU, developed in AspenOne Plus, is shown in Figure 2.

Table 2. GT modeling input data.

Parameter	Value
Ambient air temperature, °C	15
Ambient air pressure, kPa	101.3
Fuel	CH_4 (methane)
Compressor internal relative efficiency, %	88
Turbine internal relative efficiency, %	89
Combustion chamber pressure loss, %	3
Coolant flow distribution (COOLING1:COOLING2), %	70:30
Mechanical and power generator efficiency, %	99

A mathematical model of a cooled CCGT was developed using the AspenOne Plus software, which allows modeling of complex thermal schemes of power equipment. The model is represented by the following elements. The compressor is conditionally divided into 3 parts (COMP1, COMP2, COMP3), which is associated with the presence of cooling bleeds (BLEED1, BLEED2) of the gas turbine [20].

Two streams are supplied to the GTU combustion chamber (COMBCHAM)—air behind the compressor (AIR5) and fuel (FUEL). Pure methane is used as fuel.

The stoichiometric combustion of fuel occurs in the combustion chamber with subsequent chemical reactions shown in Formulas (1) and (2):

$$CH_4 + 2 \cdot O_2 = 2 \cdot H_2O + CO_2 \quad (1)$$

$$2 \cdot H_2 + O_2 = H_2O \quad (2)$$

The fuel pressure is assumed to be 30% higher than the pressure of the air entering the combustion chamber. After the combustion chamber, the gas is sent to the gas turbine, which, like the compressor, is conditionally divided into 3 parts (TURB1, TURB2, TURB3), where power is generated. COOLING1 and COOLING2 are coolant supplies, which were taken in the calculation in the ratio of 70:30 [21].

The developed mathematical model of a cooled gas turbine plant has the following assumptions:

- air extraction from the compressor does not depend on the efficiency of the applied cooling scheme, which is conditioned by the AspenOne Plus software product capabilities;
- the model does not take into account changes in the chemical composition of the working fluid;
- the model does not take into account the supply of the cooling air after each cooled nozzle and blade of the gas turbine;
- in the combustion chamber stoichiometric combustion of pure methane;
- the relative internal efficiency of the compressor, gas turbine, and losses in the combustion chamber were assumed to be constant for all considered GTU.

However, for a generalized study of the effect of cooling air flow rate on the energy characteristics of various powerful GTU and confirmation of the mathematical model operation within acceptable accuracy, these assumptions are not serious.

The total amount of cooling flow changed in the individual range adopted for each GTU. The study was carried out in order to approximate to the cooling air flow rate that could be in the design of a real foreign GTU.

The study involved well-known GTU models of foreign companies (Table 3), which have different levels of GTU electric power and different initial temperatures at the gas turbine inlet [22,23].

Table 3. Nominal characteristics of the gas turbines.

Parameter	GTU Model (Manufacturer), Parameter Value	
	GT11N2 (Alstom Power)	**SGT-1000F (Siemens)**
GT net power, MW	113.6	67.7
Pressure ratio	16	15,8
Turbine initial temperature, °C	1085	1187
Exhaust gas temperature, °C	525	537
GT net efficiency, %	33.3	35.1
GT flue gas massflow, kg/s	400	191
	PG9351 (GE)	MW701G (MHI)
GT net power, MW	256.2	334
Pressure ratio	16.6	21
Turbine initial temperature, °C	1288	1410
Exhaust gas temperature, °C	600	587
GT net efficiency, %	37.0	39.5
GT flue gas massflow, kg/s	643	750

The convergence of the results of mathematical modeling and the characteristics of real gas turbine plants was analyzed by superimposing the rated characteristics on the dependences of the change in the corresponding model characteristics on the relative coolant flow (Figures 3 and 4).

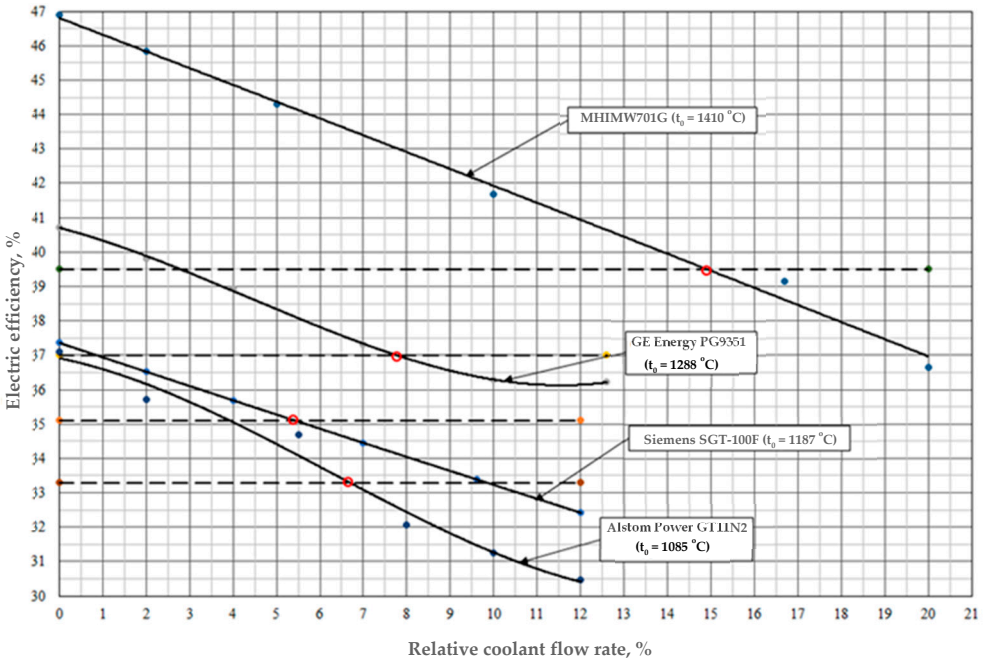

Figure 3. Dependences of changes in the electrical efficiency of GTU with different levels of power and temperatures on the relative flow rate of the coolant.

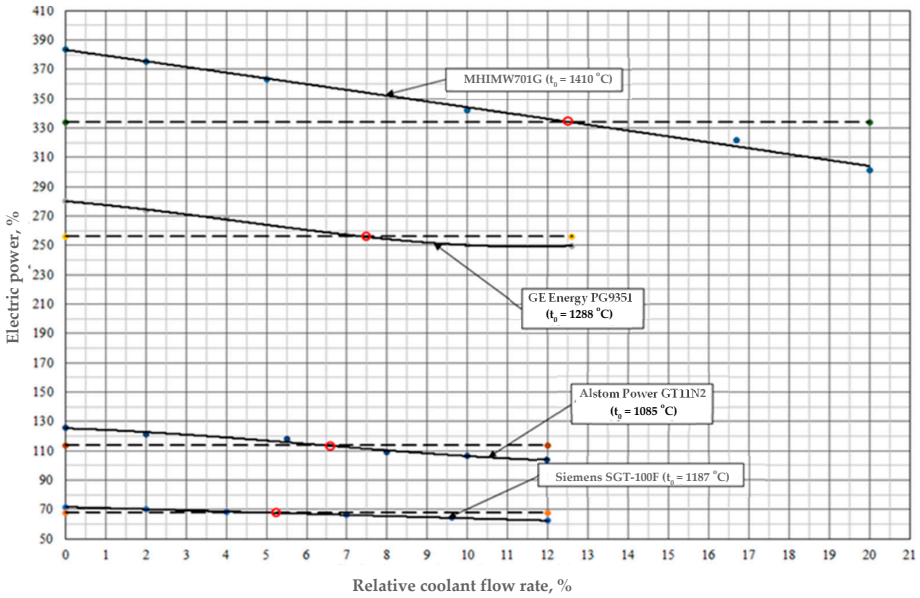

Figure 4. Dependences of changes in the electrical efficiency of GTU with different levels of power and temperatures on the relative flow rate of the coolant.

Based on the intersection points of the GTU actual rated characteristics and the dependencies obtained by cooled GTU mathematical modeling, it becomes possible to determine the approximate cooling flow rates for each of the selected units.

However, a similar procedure for comparing the temperature of the GTU exhaust gases (Figure 5), which is also the rated characteristic of the unit, gives an ambiguous nature of the dependencies, which may be caused by some assumptions that were made when developing the mathematical model. In particular, one of these assumptions is the setting of the relative internal efficiency of the gas turbine (Table 2), which directly affects the used heat drop, and, ultimately, the exhaust temperature. In addition, the dependencies of some of the GTU studied with the help of the developed model did not allow us to establish the values of the cooling rates.

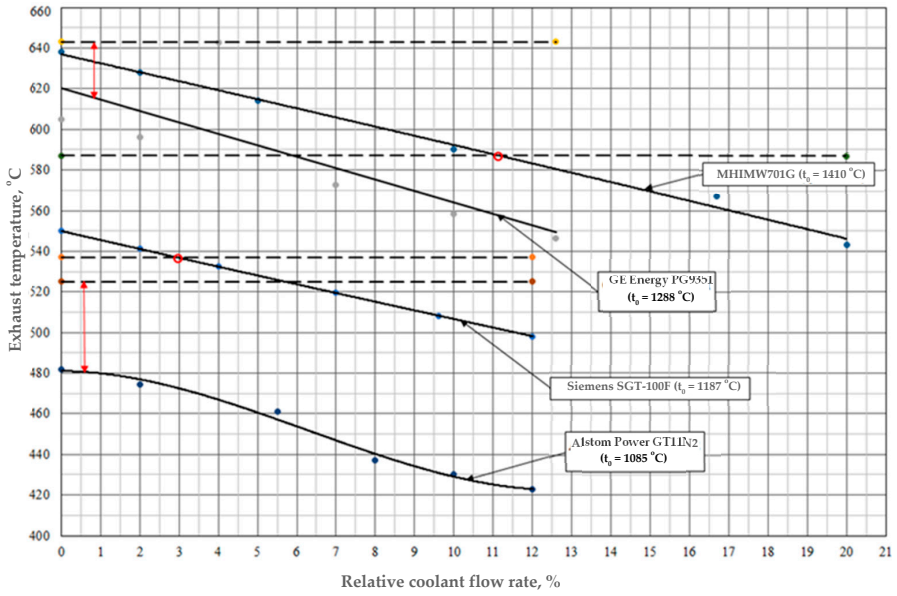

Figure 5. Dependences of temperature changes in exhaust gases of GTU with different levels of power and temperatures on the relative flow rate of the coolant.

Comparing the dependencies shown in Figure 6, it is possible to identify some relationships between the relative coolant flow rate and the initial temperature before the gas turbine. This dependence was obtained as follows: In Figure 3 (dependence of the electrical efficiency on the relative coolant flow rate for GTUs with different levels of initial temperatures before the gas turbine), the points of intersection of the characteristics plotted using the mathematical model and the GTU's rated characteristics were found (Table 3). Each intersection point had its own relative coolant flow rate, determined by projecting the intersection point onto the abscissa axis. Thus, for each GTU with its initial temperature, the corresponding value of the relative coolant flow rate by the GTU electrical efficiency was obtained, which is necessary for plotting an approximating dependence ψ_{η}. = f(t_0). The second dependence was plotted similarly—by the GTU electric power ψ_{coolN} = f(t_0). Summarizing the dependence of the relative coolant flow rate on the initial temperature before the gas turbine, averaging and subsequent extrapolation were carried out to determine ψ_{cool} at higher levels of initial temperatures.

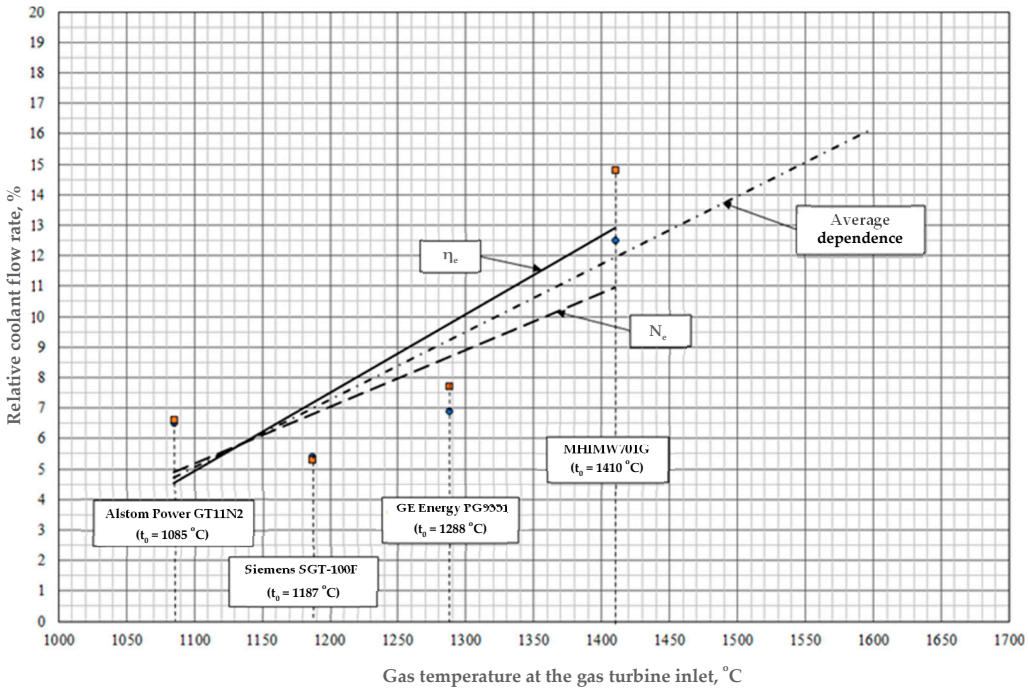

Figure 6. Dependences of temperature changes in exhaust gases of GTU with different levels of power and temperatures on the relative flow rate of the coolant.

The relationship between the relative coolant flow rate and the initial temperature before the gas turbine obtained during the study can be represented by the following empirical expression (2):

$$\psi_{cool} = 0.022 \cdot t_0 - 19, \quad (3)$$

where t_0—temperature before the gas turbine, °C.

2.3. Mathematical Models of Thermal Schemes and Methods for Calculating the Power Plants Performance Indicators

Thermodynamic studies of oxy-fuel combustion energy cycles were carried out using the AspenONE code, created to develop mathematical models of thermal circuits. The NIST REFPROP database was used to determine the thermophysical properties of liquids. The CCGT simulation model is shown in Figure 7a [24].

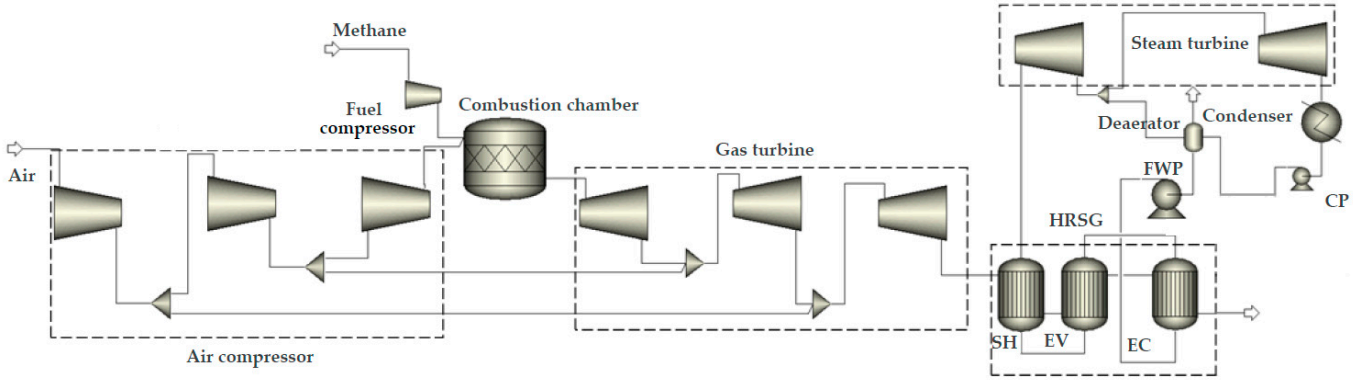

(**a**) Thermal circuit of CCGT

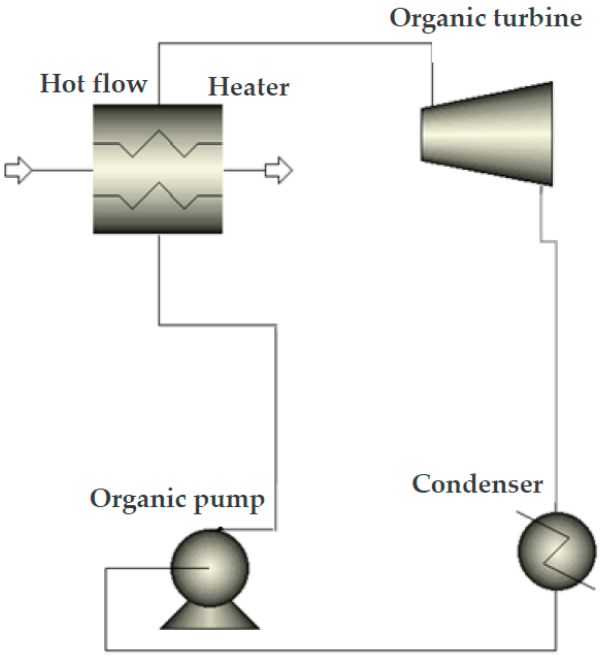

(**b**) Thermal circuit of the Rankine cycle

Figure 7. Mathematical models of thermal circuits.

During the simulation, the temperature and pressure at the inlet to the gas turbine and the air flow in the compressor were fixed. The input parameters for the ORC are presented in Table 2. A schematic diagram of the organic Rankine cycle utilizing low-grade heat is illustrated in Figure 7b.

The methodology for calculating the rest of the CCGT energy indicators was as follows. The lower heating value of the mixture is calculated by the formula:

$$LHV = \frac{NCV_{CH_4} \cdot (1-x) \cdot \frac{V_{CH_4}}{V_{H_2}+V_{CH_4}} + NCV_{H_2} \cdot x \cdot \frac{V_{H_2}}{V_{H_2}+V_{CH_4}}}{\rho_{CH_4} \cdot \frac{V_{CH_4}}{V_{H_2}+V_{CH_4}} + \rho_{H_2} \cdot \frac{V_{H_2}}{V_{H_2}+V_{CH_4}}}, \quad (4)$$

where NCV_{CH_4}—nature gas net calorific value, MJ/kg; NCV_{H_2}—hydrogen net calorific value, MJ/kg; x—volume fraction H_2; V_{CH_4}—volume flow of nature gas, m^3/s; V_{H_2}—volume flow of hydrogen, m^3/s; ρ_{CH_4}—hydrogen density, kg/m^3; ρ_{H_2}—hydrogen density, kg/m^3.

The Wobbe criterion was determined by the formula:

$$W_{ind} = \frac{LHV}{\sqrt{\frac{(1-x)\cdot\rho_{nNG}+x\cdot\rho_{nH_2}}{\rho_{nAir}}}}, \quad (5)$$

where ρ_{nNG}—nature gas density under normal conditions, kg/nm^3; ρ_{nH_2}—hydrogen density under normal conditions, kg/nm^3; ρ_{nAir}—air density under normal conditions, kg/nm^3.

Power spent for auxiliaries:

$$N_{ON} = N_{HP} + N_{LP} + N_{CEP} + N_{RP} \quad (6)$$

where N_{HP} and N_{LP}—power consumed to drive high- and low-pressure electric feed pumps, respectively; N_{CEP}—power spent on the drive of condensate electric pumps, MW; MW; N_{RP}—power consumed to drive the electric pumps for the condensate recirculation of the waste heat boiler, MW.

The net power output of GTU, STP, OCR, and CCGT was determined as

$$N^{net}_{GTU} = (N_{GT} - N_C)\cdot\eta_{EG} - N_{FC}, \quad (7)$$

$$N^{net}_{STU} = N_{ST}\cdot\eta_{EG} - N_{ON} \quad (8)$$

$$N^{net}_{OCR} = N_{OT}\cdot\eta_{EG} - N_{OP}, \quad (9)$$

$$N^{net}_{CCGT} = N^{net}_{GTU} + N^{net}_{STP} + N^{net}_{OCR}, \quad (10)$$

where N_{GT} is the power generated by the gas turbine, MW; N_c is the power consumed to drive the compressor of a gas turbine plant, MW; N_{FC} is the power consumed to fuel compressors, MW; η_{EG} is the efficiency of the electric generator, %; N_{ST} is the power generated by the steam turbine, MW; N_{OT} is the power generated by the ORC turbine, MW; and N_{OP} is the power consumed by the ORC pump, MW.

The thermal power supplied to the combustion chamber of a gas turbine plant is calculated as follows:

$$Q_{CC} = V_F\cdot LHV \quad (11)$$

where V_F is the volumetric flow rate of fuel gas under normal conditions, nm^3.

Thermal power of the waist heat boiler is determined as follows:

$$Q_b = G_{eg}\cdot(I_d - I_e) \quad (12)$$

where G_{eg} is the consumption of exhaust gases, kg/s; I_d is the enthalpy of exhaust gases at the inlet of the waste heat boiler, kJ/kg; and I_e is the enthalpy of exhaust gases at the outlet of the waste heat boiler, kJ/kg.

Waste heat boiler efficiency is as follows:

$$\eta_b = \frac{(I_d - I_e)}{(I_d - I_{outa})}, \quad (13)$$

where I_{outa} is the enthalpy of exhaust gases at an ambient air temperature of 15 °C, kJ/kg.

The net efficiencies of GTU, STP, and CCGT were determined by the formulas:

$$\eta^{net}_{GTU} = \frac{N^{net}_{GTU}}{Q_{CC}} \quad (14)$$

$$\eta^{net}_{STP} = \frac{N^{net}_{STP}}{Q_b} \quad (15)$$

$$\eta^{net}_{CCGT} = \frac{N^{net}_{CCGT}}{Q_{CC}} \quad (16)$$

3. Results and Discussion

3.1. Analysis of the Energy Performance of a Methane–Hydrogen GTU

According to the simulation results, it was found that an increase in the hydrogen content in the fuel was accompanied by a decrease in the Wobbe index and the power unit's auxiliaries (Figure 8). According to the graph (Figure 8a) it can be seen that under these conditions, without design changes, the operation of burners and nozzles in the combustion chamber can be carried out with a volume fraction of hydrogen in the fuel mixture not exceeding 80% (33% H_2 in fuel mass flow). The Wobbe index at this concentration is 43.3. With a further increase in the proportion of H_2 in the composition of the fuel, traditional burners may experience a problem with the distribution of the specific heat flow, which leads to the danger of separation and flashback of the flame at the mouth of the burner with further extinction of the torch [25]. In turn, the increase in the auxiliaries (Figure 8b) was due to an increase in the volumetric flow rate of the fuel blend, leading to an increase in the power of gas booster compressors by 2.8 MW.

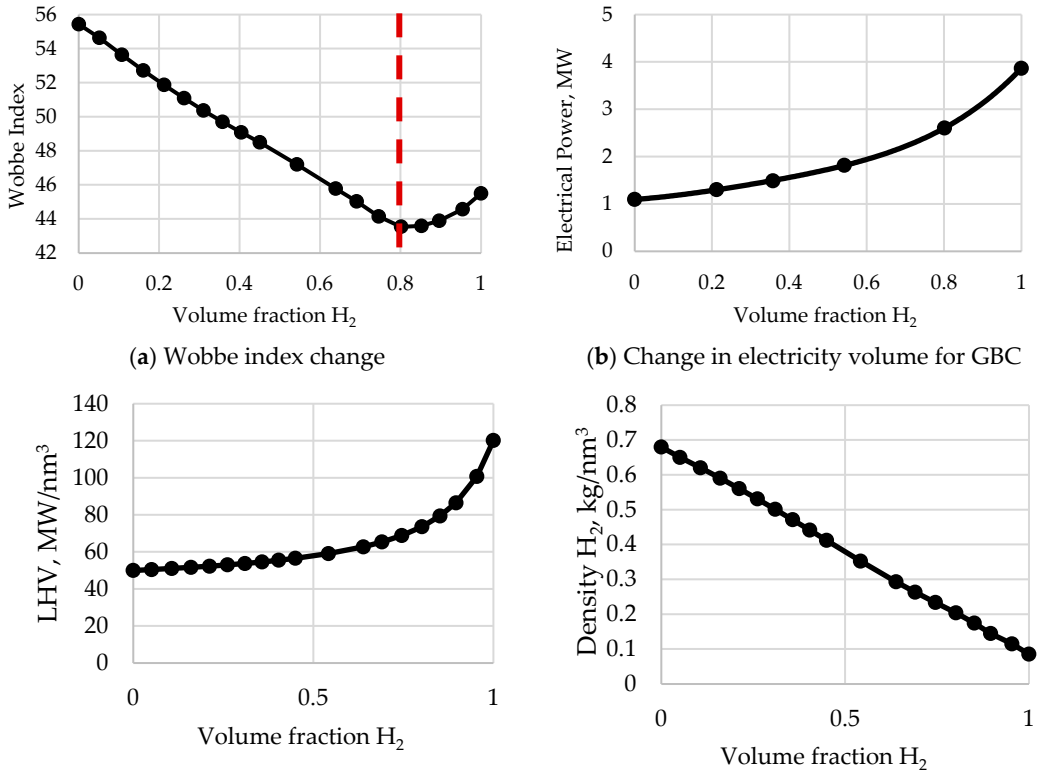

(**a**) Wobbe index change

(**b**) Change in electricity volume for GBC

(**c**) Heat power change

(**d**) Density change

Figure 8. The influence of the volume fraction of hydrogen on the performance of gas turbines.

The minimum of the Wobbe index curve is associated with the low density of hydrogen, due to which with an increase in the volume fraction of hydrogen above 80%, an intense hyperbolic increase in the volumetric thermal power occurs (Figure 9c) and a linear decrease in fuel density (Figure 9b).

It was found that with an increase in the volume content of hydrogen in the fuel mixture from 0 to 100%, the GTU output electric power increased from 315.7 to 324.8 MW (Figure 9a), and the total output power increased by 4.7 MW (Figure 9b), which was due to an increase in the heat capacity of the working fluid with an increase in the concentration of water vapor. At the same time, the net calorific value increased from 55 MW to 120 MW, and the flow rate decreased by 2.35 times, due to which the GTU net efficiency increased (Figure 9c).

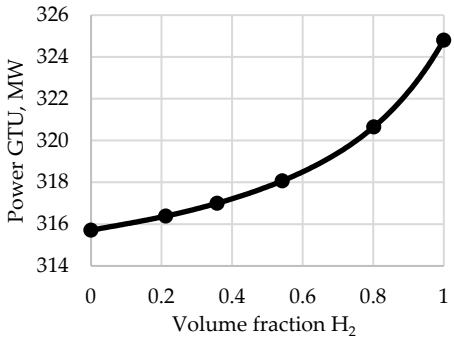

(**a**) Change gross power GTU

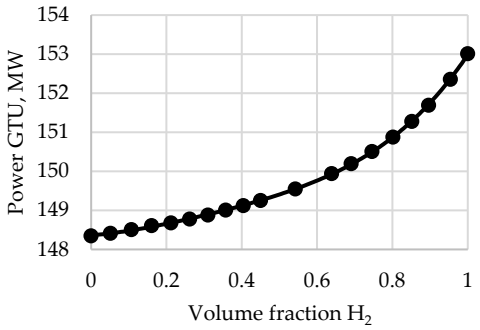

(**b**) Change net power GTU

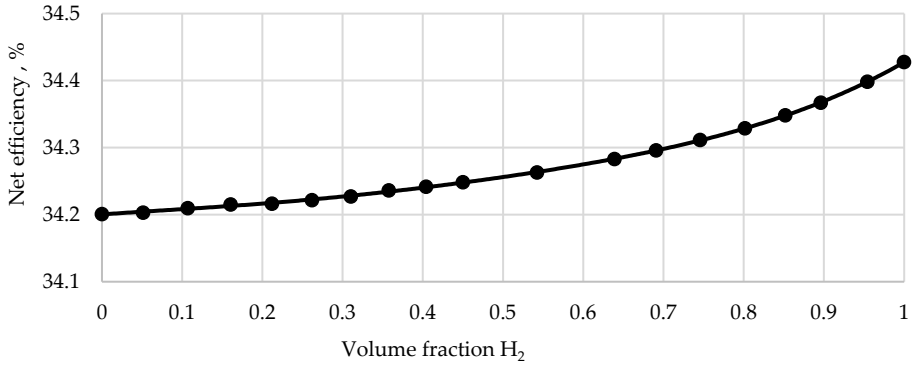

(**c**) Change in net efficiency of GTU

Figure 9. Dependence of GTU energy parameters on the volume fraction of hydrogen.

The change in gas turbine power was due to an increase in the concentration of water vapor during the combustion of H_2, which is illustrated in Figure 10a. It was found that with a change in the chemical composition from 55% to 100% of the volume fraction of hydrogen, the increase in the heat capacity of the working fluid at the gas turbine inlet was 2.5 times greater than at its outlet (Figure 10b).

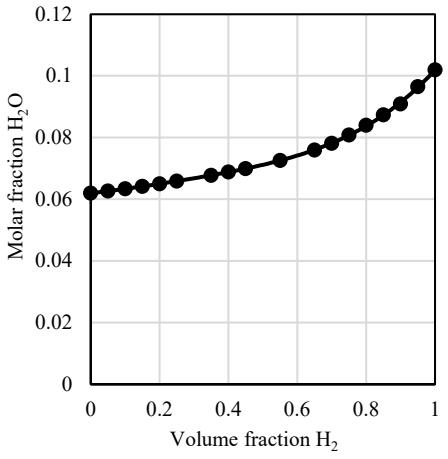

(**a**) Change in the water vapor molar fraction in the composition of the working fluid

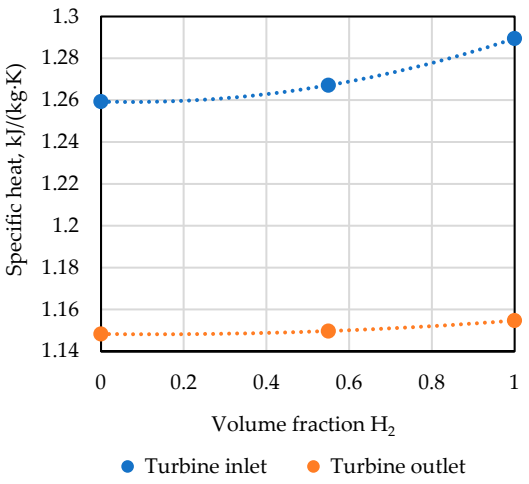

(**b**) Change in the working fluid specific heat capacity at the GT inlet and outlet

Figure 10. Influence of the volume fraction of hydrogen on the thermodynamic properties of the working fluid.

Figure 11 illustrates the effect of the methane–hydrogen blend chemical composition on the amount of carbon dioxide in the combustion products. It was revealed that the shift to hydrogen fuel completely disposed the production of electricity from carbon dioxide emissions.

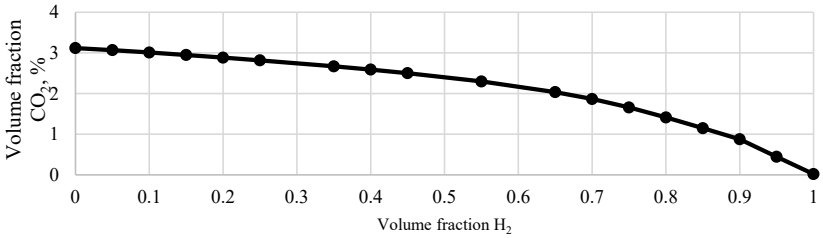

Figure 11. Effect of hydrogen volume fraction on carbon dioxide emissions.

3.2. Comparative Analysis of Energy Performance of Binary and Trinary CCGTs Operating on Methane–Hydrogen Fuel

With an increase in the volume fraction of water vapor, the volume of combustion products increased by 2.9% due to the fact that the expansion process occurred with a constant difference in entropies, and the temperature of the working fluid at the turbine outlet dropped. Figure 12a shows that an increase in the hydrogen concentration in the fuel from 0% to 100% caused a decrease in the temperature of the working fluid at the inlet to the waste heat boiler by 3.4 °C.

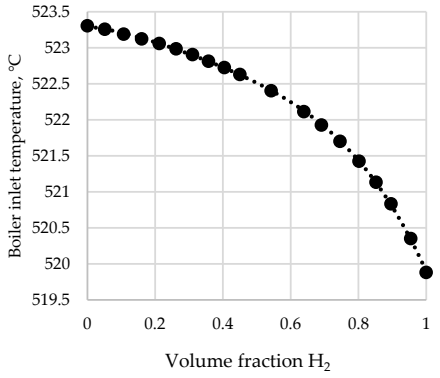

(**a**) Change in temperature of the working fluid at the GT exhaust

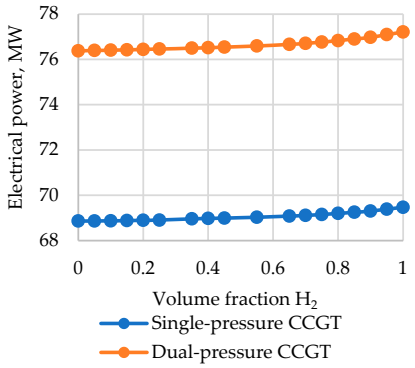

(**b**) Change in GT electric power

Figure 12. Dependence of the temperature of the working fluid and the output power on the hydrogen volume fraction.

When shifting from methane to hydrogen fuel, the amount of heat supplied to the waste heat boiler increased, due to which the consumption of water vapor and the power of the steam turbine increased by 0.8 MW (Figure 12b). It is worth noting that due to the presence of the second circuit and the condensate gas heater, the capacity of the binary CCGT unit was higher than that of the trinary unit by 7.5 MW.

The study showed (Figure 13) that the use of the organic Rankine cycle in a trinary cycle with a single-circuit waste heat boiler made it possible to generate an additional 6.3 MW of electrical energy when operating on clean natural gas. The use of hydrogen fuel increased electricity generation by 10.3 MW.

The sharp increase in electricity generation in the ORC cycle was associated with an increase in the concentration of water vapor (Figure 14a), due to which more thermal energy was released during the H_2O phase transition, which was utilized in the low-boiling cycle. However, due to technical limitations of the utilized heat exchanger, the working fluid should not have a temperature below 41.8 °C, due to which the operation of the trinary

cycle up to 75% of the content of the hydrogen volume fraction in the fuel is carried out outside the range of the water vapor condensation point (Figure 14b).

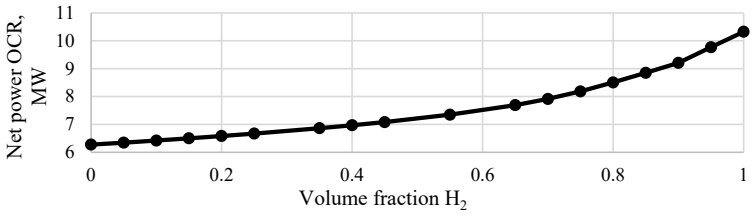

Figure 13. Dependence of the ORC output power on the hydrogen volume fraction.

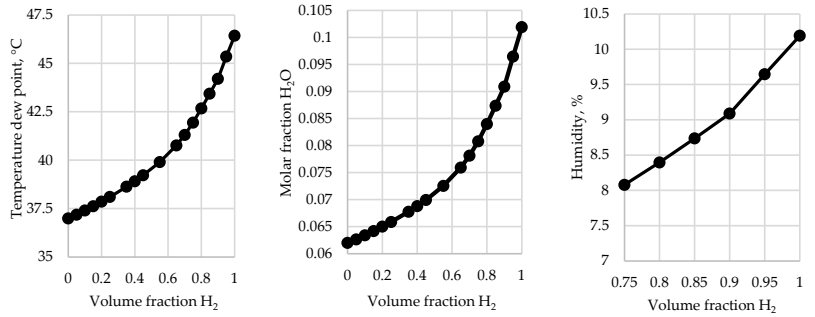

(**a**) Water vapor dew point temperature

(**b**) Volume fraction of water vapors

(**c**) Humidity of the working fluid at the outlet of the ORC

Figure 14. Thermodynamic characteristics of the working fluid at the outlet from the OCR.

With a further increase in the hydrogen concentration in the fuel, the partial pressure of water vapor increased. Due to this, after the hydrogen volume fraction in the fuel exceeded 75%, the dew point temperature reached 42 °C. The specific humidity of the exhaust gases depending on the hydrogen volume fraction in the fuel is shown in Figure 14c.

An increase in the concentration of hydrogen in the fuel increased the volume fraction of water vapor in the working fluid, which caused an increase in the heat input to the ORC and, accordingly, the generation of electricity at the plant. When comparing the efficiency of three different thermal circuits of CCGT (Figure 15), it can be seen that the greatest increase in power was observed in the trinary cycle due to the previously described phenomenon, and with an increase in the utilized energy of water vapor, the efficiency of the plant also increased.

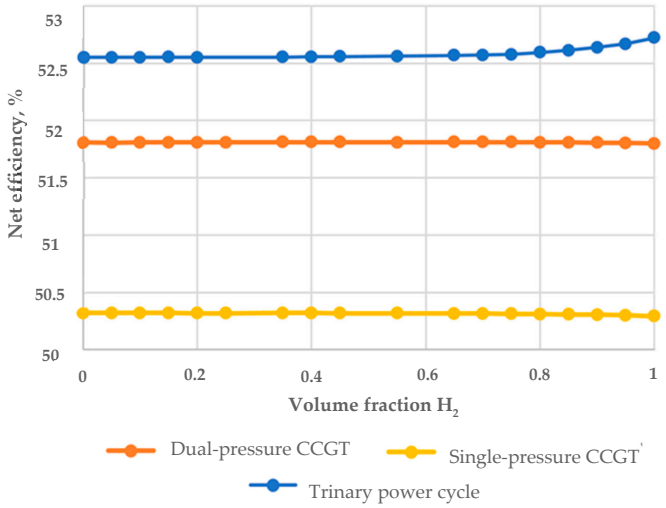

Figure 15. Comparison of energy efficiency when operating on methane–hydrogen fuel of a double-circuit and single-circuit CCGT.

4. Conclusions

This article achieved the following results:

1. For GTU-160, operation without a change of burner and nozzle design can be carried out with no more than 80% of the hydrogen volume fraction in the methane–hydrogen blend (33% of hydrogen in the fuel mass flow rate). The Wobbe index at this concentration is 43.3.
2. It was found that an increase in the hydrogen volume fraction in the fuel blend from 55% to 100% is accompanied by an increase in the content of water vapor in the composition of the working fluid. At the same time, the increase in the heat capacity of the working fluid at the inlet to the gas turbine is 2.5 times greater than at the outlet from it, which causes an increase in the heat drop in the gas turbine and an increase in the efficiency of the CHP by 0.227% relative to the GTU operating on pure natural gas.
3. With an increase in heat capacity, with an increase in the volume molar fraction of water vapor, a larger heat drop is triggered, due to which the temperature of the working fluid at the outlet of the turbine decreases by 3.4 °C when shifting from natural gas to pure hydrogen.
4. The use of ORC with the working fluid water vapor condensation allows the net efficiency to be increased by 0.74%. At the same time, when 75% of the hydrogen volume fraction is reached, a sharp increase in electricity generation in the ORC cycle occurs. This is due to the fact that the dew temperature of water vapor exceeds 42 °C at a given concentration, which causes H_2O condensation and utilization of the phase transition heat in the ORC.
5. An increase in the concentration of hydrogen in the fuel increases the mole fraction of water vapor in the working fluid, which causes an increase in the heat input to the ORC and, accordingly, the generation of electricity at the plant to 10.3 MW.

Author Contributions: Conceptualization, V.K. and N.R.; methodology, V.K. and N.R.; software, M.O.; validation, A.R. and O.Z.; formal analysis, O.Z.; investigation, M.O.; resources, O.Z.; data curation, M.O.; writing—original draft preparation, V.K.; writing—review and editing, N.R.; visualization, M.O.; supervision, A.R.; project administration, A.R.; funding acquisition, A.R. All authors have read and agreed to the published version of the manuscript.

Funding: This study conducted by the Moscow Power Engineering Institute was financially supported by the Ministry of Science and Higher Education of the Russian Federation (project no. FSWF-2020-0020).

Data Availability Statement: Not applicable.

Conflicts of Interest: The authors declare no conflict of interest.

References

1. Wang, H.; Lei, Z.; Zhang, X.; Zhou, B.; Peng, J. A review of deep learning for renewable energy forecasting. *Energy Convers. Manag.* **2019**, *198*, 111799. [CrossRef]
2. Dudin, M.N.; Frolova, E.E.; Protopopova, O.V.; Mamedov, A.A.; Odintsov, S.V. Study of innovative technologies in the energy industry: Nontraditional and renewable energy sources. *Entrep. Sustain. Issues* **2019**, *6*, 1704–1713. [CrossRef]
3. Kakoulaki, G.; Kougias, I.; Taylor, N.; Dolci, F.; Moya, J.; Jäger-Waldau, A. Green hydrogen in Europe—A regional assessment: Substituting existing production with electrolysis powered by renewables. *Energy Convers. Manag.* **2020**, *228*, 113649. [CrossRef]
4. Iida, S.; Sakata, K. Hydrogen technologies and developments in Japan. *Clean Energy* **2019**, *3*, 105–113. [CrossRef]
5. Zsiborács, H.; Baranyai, N.H.; Vincze, A.; Zentkó, L.; Birkner, Z.; Máté, K.; Pintér, G. Intermittent renewable energy sources: The role of energy storage in the european power system of 2040. *Electronics* **2019**, *8*, 729. [CrossRef]
6. Terlouw, T.; AlSkaif, T.; Bauer, C.; Sark, W. Optimal energy management in all-electric residential energy systems with heat and electricity storage. *Appl. Energy* **2019**, *254*, 113580. [CrossRef]
7. Chapman, A.; Itaoka, K.; Hirosea, K.; Davidson, T.; Nagasawa, K.; Lloyd, A.; Webber, M.; Kurban, Z.; Managie, S.; Tamaki, T.; et al. A review of four case studies assessing the potential for hydrogen penetration of the future energy system. *Int. J. Hydrog. Energy* **2019**, *44*, 6371–6382. [CrossRef]
8. Abe, J.O.; Popoola, A.P.I.; Ajenifuja, E.; Popoola, O.M. Hydrogen energy, economy and storage: Review and recommendation. *Int. J. Hydrog. Energy* **2019**, *44*, 15072–15086. [CrossRef]

9. Ali, L.M.; Ali, Q.A.; Klačková, I.; Issa, H.A.; Yakimovich, B.A.; Kuvshimov, V. Developing a thermal design for steam power plants by using concentrating solar power technologies for a clean environment. *Acta Montan. Slovaca* **2021**, *26*, 773–783.
10. Moradi, R.; Groth, K.M. Hydrogen storage and delivery: Review of the state of the art technologies and risk and reliability analysis. *Int. J. Hydrog. Energy* **2019**, *44*, 12254–12269. [CrossRef]
11. Timmerberg, S.; Kaltschmitt, M. Hydrogen from renewables: Supply from North Africa to Central Europe as blend in existing pipelines–Potentials and costs. *Appl. Energy* **2019**, *237*, 795–809. [CrossRef]
12. Bassily, A. Enhancing the Efficiency and Power of the Triple-Pressure Reheat Combined Cycle by Means of Gas Reheat, Gas Recuperation, and Reduction of the Irreversibility in the Heat Recovery Steam Generator. *Appl. Energy* **2008**, *85*, 1141–1162. [CrossRef]
13. Bassily, A. Modeling, Numerical Optimization, and Irreversibility Reduction of a Dual-Pressure Reheat Combined-Cycle. *Appl. Energy* **2005**, *81*, 127–151. [CrossRef]
14. Hada, S.; Yuri, M.; Masada, J.; Ito, E.; Tsukagoshi, K. Evolution and Future Trend of Large Frame Gas Turbines: A New 1600 °C, J Class Gas Turbine. In *Turbo Expo: Power for Land, Sea, and Air*; American Society of Mechanical Engineers: Copenhagen, Denmark, 2012; pp. 599–606.
15. Protalinsky, O.M.; Shcherbatov, I.A.; Stepanov, P.V. Identification of the actual state and entity availability forecasting in power engineering using neural-network technologies. *J. Phys. Conf. Ser.* **2017**, *891*, 012289. [CrossRef]
16. Rogalev, A.; Rogalev, N.; Kindra, V.; Zlyvko, O.; Vegera, A. A Study of Low-Potential Heat Utilization Methods for Oxy-Fuel Combustion Power Cycles. *Energies* **2021**, *14*, 3364. [CrossRef]
17. Rogalev, N.; Kindra, V.; Komarov, I.; Osipov, S.; Zlyvko, O.; Lvov, D. Comparative Analysis of Low-Grade Heat Utilization Methods for Thermal Power Plants with Back-Pressure Steam Turbines. *Energies* **2021**, *14*, 8519. [CrossRef]
18. Galashov, N.; Tsibulskiy, S.; Serova, T. Analysis of the Properties of Working Substances for the Organic Rankine Cycle Based Database "REFPROP". *EPJ Web Conf.* **2016**, *110*, 01068. [CrossRef]
19. Kindra, V.; Rogalev, N.; Osipov, S.; Zlyvko, O.; Naumov, V. Research and Development of Trinary Power Cycles. *Inventions* **2022**, *7*, 56. [CrossRef]
20. Canie're, H.; Willockx, A.; Dick, E.; De Paepe, M. Raising cycle efficiency by intercooling in air-cooled gas turbines. *Appl. Therm. Eng.* **2006**, *26*, 1780–1787. [CrossRef]
21. Shevchenko, I.V.; Rogalev, A.N.; Shevchenko, M.I.; Strogonova, L.B.; Yaropolov, V.I. Application of additive laser technologies for full-scale modeling in the design of cooled gas turbine blades. *Int. J. Mech. Eng. Technol.* **2018**, *9*, 2097–2105.
22. Trukhny, A.D. *Combined-Cycle Plants of Power Plants: A Textbook for Universities*; MPEI Publishing House: Moscow, Russia, 2017; p. 675.
23. The Basic Technical Characteristics of GTUs and CCGTs of Foreign Companies. Reference Summary of the Discipline Sources and Systems of Heat Supply of Enterprises. Available online: https://vunivere.ru/work33768/page29 (accessed on 6 November 2020).
24. Helvensteijn, B.P.; Wang, Y.; Levan, D.; Luna, B.; Kashani, A. Adsorption of oxygen onto zeolites at pressures up to 15 MPa. *AIP Conf. Proc.* **2012**, *1434*, 1245–1252.
25. Zhao, Y.; McDonell, V.; Samuelsen, S. Influence of hydrogen addition to pipeline natural gas on the combustion performance of a cooktop burner. *Int. J. Hydrog. Energy* **2019**, *44*, 12239–12253. [CrossRef]